JACS
JOURNAL OF THE AMERICAN CHEMICAL SOCIETY
Article
pubs.acs.org/JACS

High-Performance Solution-Processed Non-Fullerene Organic Solar Cells Based on Selenophene-Containing Perylene Bisimide Acceptor

Dong Meng,[†,‡,§] Dan Sun,[†,‡,§] Chengmei Zhong,[∥,⊥] Tao Liu,[†] Bingbing Fan,[†] Lijun Huo,[†] Yan Li,[‡] Wei Jiang,[‡] Hyosung Choi,[#] Taehyo Kim,[▽] Jin Young Kim,[▽] Yanming Sun,*[,†] Zhaohui Wang,*[,‡] and Alan J. Heeger[†,⊥]

[†]Heeger Beijing Research and Development Center, School of Chemistry and Environment, Beihang University, Beijing 100191, PR China

[‡]Beijing National Laboratory for Molecular Science, Key Laboratory of Organic Solids, Institute of Chemistry, Chinese Academy of Sciences, Beijing 100190, PR China

[§]University of Chinese Academy of Sciences, Beijing 100049, PR China

[∥]State Key Laboratory of Luminescent Materials and Devices, South China University of Technology, Guangzhou 510641, PR China

[⊥]Center for Polymers and Organic Solids, University of California, Santa Barbara, California 93106, United States

[#]Department of Chemistry and Institute for Materials Design, Hanyang University, Seoul 133-791, South Korea

[▽]School of Energy and Chemical Engineering, Ulsan National Institute of Science and Technology (UNIST), Ulsan 689-798, South Korea

Supporting Information

ABSTRACT: Non-fullerene acceptors have recently attracted tremendous interest because of their potential as alternatives to fullerene derivatives in bulk heterojunction organic solar cells. However, the power conversion efficiencies (PCEs) have lagged far behind those of the polymer/fullerene system, mainly because of the low fill factor (FF) and photocurrent. Here we report a novel perylene bisimide (PBI) acceptor, SdiPBI-Se, in which selenium atoms were introduced into the perylene core. With a well-established wide-band-gap polymer (PDBT-T1) as the donor, a high efficiency of 8.4% with an unprecedented high FF of 70.2% is achieved for solution-processed non-fullerene organic solar cells. Efficient photon absorption, high and balanced charge carrier mobility, and ultrafast charge generation processes in PDBT-T1:SdiPBI-Se films account for the high photovoltaic performance. Our results suggest that non-fullerene acceptors have enormous potential to rival or even surpass the performance of their fullerene counterparts.

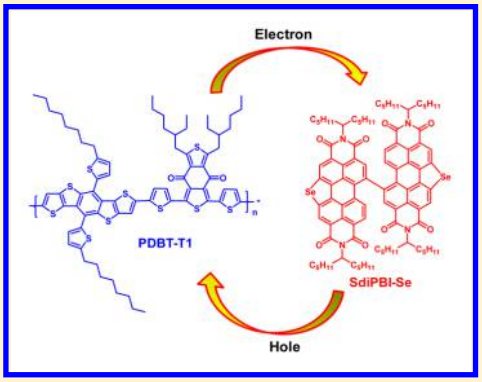

INTRODUCTION

Organic solar cells represent a relatively new approach to exploiting solar energy because of their attractive features, such as low cost, light weight, and flexibility for large-area fabrication.[1−3] Bulk heterojunction (BHJ) polymer solar cells (PSCs) typically comprise a polymer donor and a fullerene derivative acceptor, the state-of-the-art single-junction devices of which have been reported to reach 9−11% power conversion efficiencies (PCEs).[4−9] Although such PSCs achieved success in academic laboratories, they are not the ideal candidates for practical applications because the production of fullerenes is very expensive and because the chemical modification of fullerenes remains challenging.[10−13] On the contrary, non-fullerene acceptors have the advantages of low cost, synthetic versatility, strong absorption ability, and high environmental/thermal stability and have recently emerged as a hot area of focus in the field of organic photovoltaics.[14−18] At first, the performance of non-fullerene PSCs lagged far behind the corresponding PSCs mainly because of low short-circuit current (J_{sc}) and fill factor (FF).[19−22] However, several excellent polymer/non-fullerene systems have emerged in the last two years, leading to the high PCEs over 6%.[23−28] Rapid progress in PCEs indicates that non-fullerene organic solar cells have enormous potential to approach performance similar to that of fullerene-based solar cells.

Solution-processed non-fullerene acceptors can be divided into two classes: small molecules and polymers.[29−32] Compared to polymer acceptors, small-molecule acceptors possess the advantages of well-defined molecular structure, higher purity, and better batch-to-batch reproducibility. Despite these advantages, organic solar cells based on small molecule acceptors tend to show relatively low PCEs (<7%). Very recently, we have reported a bay-linked perylene bisimide (PBI)

Received: October 25, 2015

DOI: 10.1021/jacs.5b11149
J. Am. Chem. Soc. XXXX, XXX, XXX−XXX

dimer, in which sulfur atoms were incorporated into the perylene core. PSCs based on SdiPBI-S acceptor show a high PCE of 7.16%.[33] Given the similarity between thiophene and selenophene rings, the high performance of SdiPBI-S inspired us continuously to develop its selenophene analogue. Selenium has a bigger and looser outmost electron cloud than that of sulfur, which improves orbital overlap and increases the charge carrier mobility. In addition, the empty orbital on selenium can also enhance the electron-accepting ability of the parent carbon skeleton. It can facilitate fine-tuning of the electronic structure and optical band gap of parent core. Meanwhile, selenophene compounds are expected to increase intramolecular interactions because the selenium atom is more easily polarized than sulfur atom.[34−38]Accordingly, it is rational to design and synthesize selenophene compounds to investigate extensively their application in organic photovoltaics.

In this study, a novel selenophene-containing PBI acceptor, SdiPBI-Se, was synthesized. The introduction of selenium atom to the PBI core results in a high lowest unoccupied molecular orbital (LUMO) level of −3.87 eV, a twisted molecular configuration, and a high electron mobility of 6.4×10^{-3} cm^2 V^{-1} s^{-1}. The main absorptions of SdiPBI-Se are in the wavelength range of 400−600 nm. By incorporating a well-established polymer donor, PDBT-T1,[4] organic solar cells based on SdiPBI-Se show a high efficiency of 8.4%, with an open-circuit voltage (V_{oc}) of 0.96 V, a J_{sc} of 12.49 mA cm^{-2}, and an unprecedented high FF of 70.2%. This performance is comparable to that of PDBT-T1:PC_{70}BM solar cells (PCE = 8.5%) under similar fabrication conditions. To the best of our knowledge, the resulting PCE of 8.4% is among the highest values reported in the literature so far for solution-processed non-fullerene organic solar cells. The high performance is due to the synergistic effects of efficient photon absorption, high and balanced charge carrier mobility, and ultrafast charge generation. Our results provide important progress for non-fullerene organic solar cells, rendering them more competitive compared to fullerene-based solar cells.

RESULTS AND DISCUSSION

The chemical structures of PDBT-T1 and SdiPBI-Se are shown in Figure 1a. The synthesis of SdiPBI-Se is shown in Scheme 1.

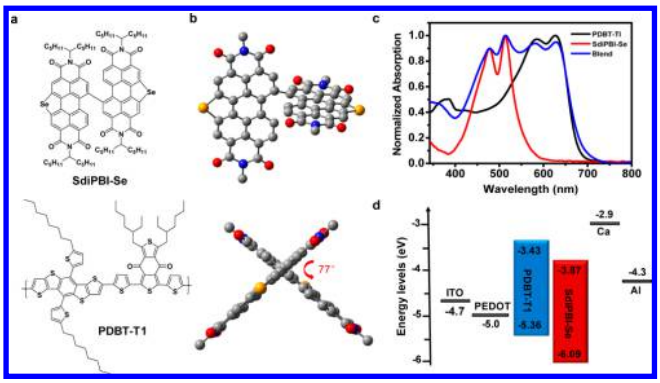

Figure 1. (a) Chemical structures of SdiPBI-Se and PDBT-T1. (b) Side and top views of the optimized geometry of SdiPBI-Se by using DFT calculations at the B3LYP/6-31G(d) level. To simplify the calculation, the alkyl side chains were replaced by methyl groups. (c) Normalized UV−vis absorption spectra of neat SdiPBI-Se, PDBT-T1, and PDBT-T1:SdiPBI-Se blend (1:1, w/w) films. (d) Energy levels of diagrams of all materials used in the solar cell device.

Scheme 1. Synthetic Route of SdiPBI-Se

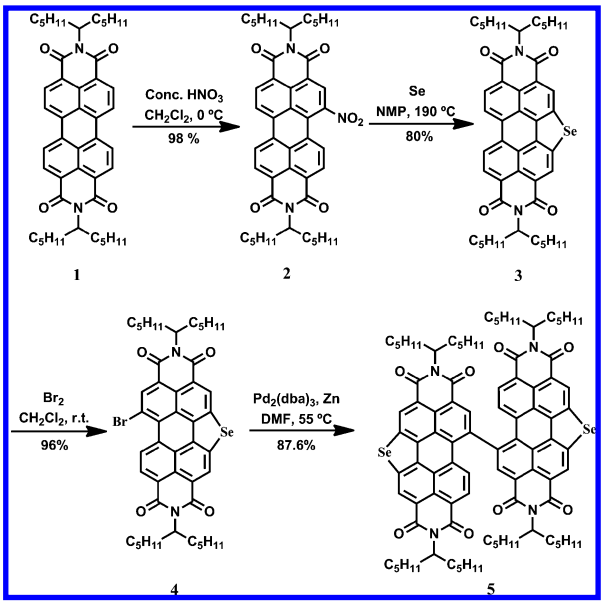

Se-annulated monomer PBI was prepared in high yield by a surprisingly simple one-pot procedure from the readily available precursor 1-nitroperylene bisimide **2** that was synthesized by nitrification of monomer perylene bisimide **1** at 0 °C. The key step was carried out in *N*-methylpyrrolidone (NMP) with selenium powder at 190 °C in 30 min following purification by column chromatography to give desired heteroatom-annulated product **3**. Subsequent key intermediate **4** was synthesized by bromination of compound **3** under dichloromethane at room temperature in 2 h. Then, treatment of compound **4** with $Pd_2(dba)_3$ and zinc powder as the catalyst underwent homocoupling at 55 °C in 1 h, directly affording product **5** in high yield. Compared to our previous synthesis route,[33] this highly effective practical strategy avoids using corrosive concentrated acid and toxic organotins reagent. The compounds were characterized by ^1H and ^{13}C NMR spectra.

The optimized geometry of SdiPBI-Se was calculated by using the density functional theory (DFT) at the B3LYP/6-31G(d) level. As illustrated in Figure 1b, the dihedral angel between the two PBI units is 77°, indicating that the molecular structure of SdiPBI-Se is largely twisted owing to the selenium bridge that reduces the flexibility of configuration change and thus increases the steric repulsion of PBI units. In dilute chloroform solution, SdiPBI-Se exhibits strong absorption in the wavelength range of 400−600 nm with a maximum extinction coefficient of 1.04×10^5 M^{-1} cm^{-1} at 510 nm. The maximum absorption coefficient of SdiPBI-Se in film is 47 537 cm^{-1} at 474 nm, indicative of its strong light-absorbing capability (Figure S1). Compared to SdiPBI-Se in solution, neat SdiPBI-Se film shows similar absorption spectra, indicative of weak aggregation in the solid state. The main absorption of PDBT-T1 is in the spectral range of 500−700 nm, complementary to the absorption spectrum of SdiPBI-Se. As a result, broad absorption in the visible range of 400−700 nm was clearly seen for PDBT-T1:SdiPBI-Se blend film (1:1, w/w). Both absorption characters of PDBT-T1 and SdiPBI-Se contributed to the enhanced light harvesting in the visible spectrum. The optical bandgap of SdiPBI-Se estimated from the absorption edge is 2.22 eV. Photoluminescence (PL) properties of PDBT-T1, SdiPBI-Se, and the 1:1 blend films

DOI: 10.1021/jacs.5b11149
J. Am. Chem. Soc. XXXX, XXX, XXX−XXX

Table 1. Summary of Device Parameters of PDBT-T1:SdiPBI-Se Solar Cells with Different DIO Concentrations under Simulated AM 1.5G (100 mW cm^{-2})

DIO (%)	V_{oc} (V)	J_{sc} (mA/cm^2)	FF (%)	PCE (%)[a]	PCE$_{max}$ (%)
0	0.949 ± 0.002	11.55 ± 0.29	67.4 ± 0.8	7.39 ± 0.29	7.55
0.25	0.947 ± 0.009	12.48 ± 0.09	69.7 ± 0.8	8.23 ± 0.08	8.42
0.5	0.938 ± 0.003	11.10 ± 0.14	68.9 ± 0.7	7.19 ± 0.07	7.23
1.0	0.918 ± 0.002	9.03 ± 0.04	67.3 ± 0.5	5.58 ± 0.04	5.63

[a]The average PCE value was calculated from six devices for each condition.

were measured (Figure S2). Compared to the PL of the neat and blend films, nearly complete quenching (>98%) of both the neat PDBT-T1 and SdiPBI-Se emissions was seen in the 1:1 blend films, indicating highly efficient charge transfer between PDBT-T1 and SdiPBI-Se. Electrochemical cyclic voltammetry (CV) was used to investigate the energy levels of SdiPBI-Se (Figure S3). The LUMO value of SdiPBI-Se is estimated to be −3.87 eV from the onset reduction potential. The high LUMO energy level results from the strong electron-donating ability of selenium atom.

To evaluate the photovoltaic performance of SdiPBI-Se, conventional solar cells were fabricated with the device configuration of ITO/PEDOT:PSS/PDBT-T1:SdiPBI-Se/Ca/Al, where ITO is indium tin oxide, PEDOT is poly(3,4-ethylenedioxythiophene), and PSS is poly(styrenesulfonate). The photovoltaic performance of solar cells fabricated under different conditions is summarized in Tables 1 and S1, and the current density−voltage (J−V) characteristics of devices are shown in Figures 2a and S4. The optimal weight ratio of

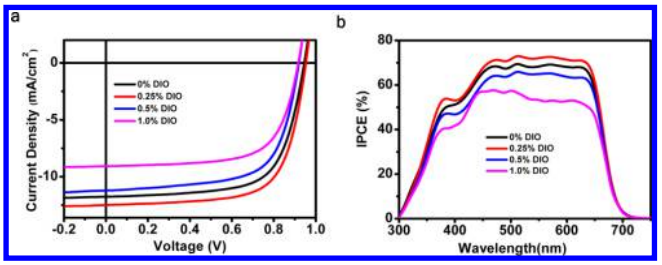

Figure 2. (a) J−V curves of PDBT-T1:SdiPBI-Se solar cells with different DIO concentrations under simulated AM 1.5G irradiation (100 mW cm^{-2}) and (b) the corresponding IPCE spectra.

PDBT-T1 and SdiPBI-Se was found to be 1:1. At this blend ratio, PDBT-T1:SdiPBI-Se solar cells exhibit remarkable high PCEs of 7.55%, with V_{oc} of 0.95 V, J_{sc} of 11.75 mA cm^{-2}, and FF of 67.8% without any additives. To improve further the PCE, 1,8-diiodooctane (DIO) was used as the processing additive. The effect of DIO concentration on the performance enhancement of solar cells was investigated. It is noted that at a DIO concentration of 0.25% J_{sc} and FF were both increased resulting in a high PCE of 8.42% with V_{oc} of 0.96 V, J_{sc} of 12.49 mA cm^{-2}, and FF of 70.2%. The average efficiency is 8.23% over six devices. Further increasing the concentration of DIO led to an efficiency reduction. For example, when the DIO concentration was raised to 0.5%, the efficiency decreased to 7.23%. The J_{sc} dropped off from 12.49 to 11.10 mA cm^{-2}. As the DIO concentration increased to 1%, a significant decrease in J_{sc} was observed, causing reduced efficiencies (5.63%). Accordingly, the champion solar cell was obtained at the DIO concentration of 0.25%, with a high PCE of 8.42% and a high FF of 70.2%. To the best of our knowledge, this efficiency is among the highest values for solution-processed non-fullerene organic solar cells so far. The unprecedented high FF of 70.2% is also the record FF value for non-fullerene organic solar cells and is also among the highest FF values for polymer−fullerene BHJ solar cells. It is noted that the PCE of solar cells slightly decreased with the increase of the active layer thickness. At a thickness of 170 nm, the PCE of solar cells was 7.21% (Table S2). The corresponding incident photon conversion efficiency (IPCE) plots of solar cells are displayed in Figure 2b. Solar cells based on the combination of PDBT-T1 and SdiPBI-Se yielded broad IPCE spectra from 300 to 700 nm, with the maximum peak up to 73.3% at 510 nm for the champion cell. The calculated J_{sc} integrated from the IPCE was 12.31 mA cm^{-2}, similar to that measured from the J−V curves with a 1.4% mismatch. In addition, fullerene-based solar cells with PDBT-T1 were also fabricated for comparison. Under similar conditions (chlorobenzene as the host solvent and 3% DIO as the additive), PDBT-T1:PC$_{70}$BM solar cells show a high PCE of 8.47%, with V_{oc} of 0.91 V, J_{sc} of 12.75 mA cm^{-2}, and FF of 73.1% (Figure S5). This performance is very comparable to that of PDBT-T1: SdiPBI-Se solar cells.

The bulk charge-transport properties of PDBT-T1:SdiPBI-Se blend films were investigated by using the space-charge-limited current (SCLC) method.[39] The device structures for hole-only and electron-only measurements were ITO/MoOx/PDBT-T1:SdiPBI-Se/MoOx/Al and ITO/Al/PDBT-T1:SdiPBI-Se/Al, respectively. Nearly balanced charge transport was found with hole mobility of 3.6 × 10^{-3} cm^2 V^{-1} s^{-1}, and the electron mobility of 4.8 × 10^{-3} cm^2 V^{-1} s^{-1}, respectively ($\mu e/\mu h$ = 1.3, Figure S6). The electron mobility of neat SdiPBI-Se film is 6.4 × 10^{-3} cm^2 V^{-1} s^{-1} (Figure S7). The high mobility is probably ascribed to the loose electron cloud of the outmost p orbital of selenium, which improves the interactions between Se−Se atoms, facilitating electron transport.[40] The high charge carrier mobility and balanced carrier transport would partially explain the high PCEs and high FF observed in the devices.

The morphologies of PDBT-T1:SdiPBI-Se blend films were studied using atomic force microscopy (AFM). As shown in Figure S8, the film processed without DIO presents uniform and fibrous features with a root-mean-square (RMS) roughness of 1.54 nm. With regard to the optimal active layer (0.25% DIO), the fibrous feature still remains apparent, but the film becomes slightly rougher with a RMS value of 1.84 nm. The height images of neat PDBT-T1 films and PDBT-T1:SdiPBI-Se films with 0.25% DIO were also measured for comparison. In terms of PDBT-T1 films, the fibrous features are still seen with increased RMS values from 1.37 to 1.67 nm after the addition of DIO, similar to those of the blend films. For SdiPBI-Se films, quite smooth and uniform surfaces were observed with a RMS value of 0.51 nm. DIO did not change the surface properties because there is no apparent aggregation within the films. The results suggest that DIO induced the aggregation of PDBT-T1 in blend films which was also confirmed by grazing incidence wide-angle X-ray scattering (GIWAXS) measurements.

DOI: 10.1021/jacs.5b11149
J. Am. Chem. Soc. XXXX, XXX, XXX−XXX

GIWAXS analysis was performed to gain insight into the crystallinity and molecular orientation of the active layer.[41] Figure 3 presents the 2D GIWAXS patterns of both neat and

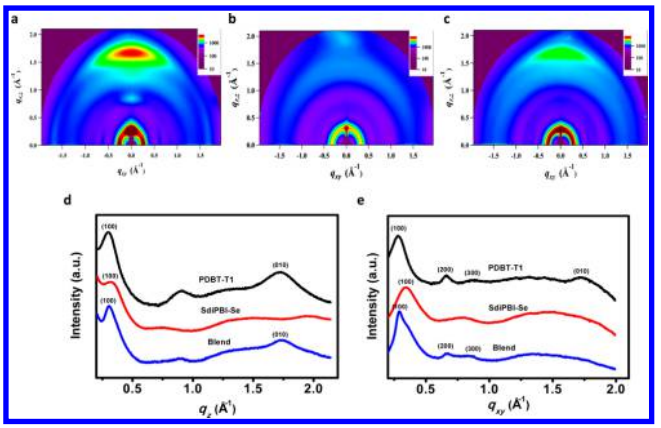

Figure 3. 2D GIWAXS patterns of (a) neat PDBT-T1 film, (b) neat SdiPBI-Se film, and (c) optimal PDBT-T1:SdiPBI-Se blend film (0.25% DIO). (d) Out-of-plane and (e) in-plane line cuts from 2D GIWAXS patterns.

BHJ blend films with the corresponding out-of-plane and in-plane line cuts. For the PDBT-T1 neat film, Bragg reflections arise from q_z = 0.296 and 1.71 nm^{-1}, which correspond to the formation of a lamellar structure (d = 21.21 Å) and $\pi-\pi$ stacking (d = 3.67 Å). The lamellar (100), (200), and (300) reflection peaks indicate the presence of crystalline domains of PDBT-T1. The observation of (010) $\pi-\pi$ stacking peak along with the multiple diffraction patterns in the in-plane direction indicates the coexistence of edge-on and face-on polymer backbone orientation. The lamellar (100) peak of SdiPBI-Se is located at 0.318 nm^{-1} with d spacing of 19.74 Å. The absence of (010) $\pi-\pi$ stacking peak for SdiPBI-Se neat film is due to the twisted molecular configuration, which prevents $\pi-\pi$ stacking of the PBI cores. Compared to the neat film, the lamellar (100), (200), and (300) reflection peaks of PDBT-T1 in BHJ films with 0.25% DIO were also found; however, the (010) $\pi-\pi$ stacking peak disappeared in the in-plane direction. Instead, a strong (010) $\pi-\pi$ stacking peak (q_z = 1.74 nm^{-1}) was seen in the out-of-plane direction, suggesting that the polymer had a preferred face-on orientation relative to the substrate. No distinct lamellar peak of SdiPBI-Se was seen in BHJ films, indicating that SdiPBI-Se should mix well with PDBT-T1. Clearly, the addition of a small amount of DIO additive (0.25%) into the casting solutions promotes the face-on orientation in films, which is beneficial for vertical charge transport, leading to a high efficiency.

Femtosecond transient absorption spectroscopy (TAS) technique was carried out to investigate the charge generation process and recombination dynamics of PDBT-T1:SdiPBI-Se blend films.[42−44] As mentioned above, PDBT-T1:$PC_{70}BM$ solar cells show high photovoltaic performance. Here, PDBT-T1:$PC_{70}BM$ blend films were also measured for comparison. Two distinct pump wavelengths were applied to excite the BHJ thin films: 488 nm to excite both the polymer donor and acceptor and 643 nm to excite only the polymer donor. The TAS spectra of PDBT-T1:$PC_{70}BM$ and PDBT-T1:SdiPBI-Se films under different pump wavelengths are shown in Figure 4a. The photoinduced absorption features from 750 to 850 nm correspond to charge absorption in PDBT-T1 (determined by

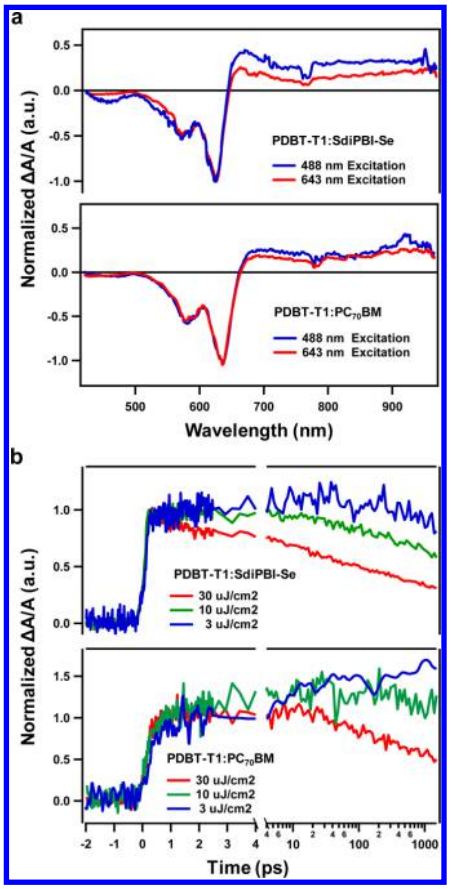

Figure 4. (a) Normalized TAS spectra of PDBT-T1:SdiPBI-Se and PDBT-T1:$PC_{70}BM$ thin films at time delay of 1 ps and excitation wavelength of 488 or 643 nm. (b) Pump-intensity-dependent charge population dynamics at excitation wavelength of 488 nm (dynamics extracted at 820 nm) of PDBT-T1:SdiPBI-Se and PDBT-T1:$PC_{70}BM$ thin films.

comparison of TAS spectra of BHJ sample and pristine PDBT-T1 sample in Figure S9). As seen in Figure 4a, the charge absorption signal is significantly stronger in 488 nm excitation compared to 643 nm excitation for the PDBT-T1:SdiPBI-Se sample. For the PDBT-T1:$PC_{70}BM$ sample, the charge absorption signal remains similar under different pump wavelengths. This suggests that both donor and acceptor contribute to overall photocurrent generation in PDBT-T1:SdiPBI-Se blend, whereas in PDBT-T1:$PC_{70}BM$ blend, the donor dominates photocurrent generation, agreeing well with the fact that SdiPBI-Se has superior absorption behavior over $PC_{70}BM$ in the visible wavelength region.

The pump intensity dependence of the charge generation of PDBT-T1:$PC_{70}BM$ and PDBT-T1:SdiPBI-Se films are compared within the time window of the TAS measurements (from 160 fs to 1.5 ns). The charge population dynamics were extracted at 820 nm in the TAS spectrum to minimize the influence of stimulated emission and exciton absorption. It is clearly seen from Figure 4b that both PDBT-T1:$PC_{70}BM$ and PDBT-T1:SdiPBI-Se films displayed an ultrafast charge generation process that saturates within the time resolution of the TAS setup (160 fs), consistent with previous findings in high-performance BHJ systems. The results suggest that either the degree of exciton delocalization or charge delocalization[45] is similar in SdiPBI-Se and $PC_{70}BM$. In contrast, the slow charge generation processes at longer time scales (>1 ps) in PDBT-

DOI: 10.1021/jacs.5b11149
J. Am. Chem. Soc. XXXX, XXX, XXX−XXX

T1:$PC_{70}BM$ are caused by the exciton dissociation process, which is remarkably different from PDBT-T1:SdiPBI-Se. At the lowest pump intensity of 3 $\mu J/cm^2$, the slow charge generation contributed up to 30% of total charge population in PDBT-T1:$PC_{70}BM$, whereas in PDBT-T1:SdiPBI-Se this number is less than 10%. This means that BHJ films with SdiPBI-Se would rely more on the ultrafast charge generation process to produce photocurrent than those of $PC_{70}BM$ which could potentially increase photocurrent generation in SdiPBI-Se because ultrafast charge generation process is less likely to result in losses from geminate recombination[46] and complicated CT state interactions.[47,48] However, this advantage is offset by the relatively stronger charge recombination in PDBT-T1:SdiPBI-Se compared to that in PDBT-T1:$PC_{70}BM$. Both BHJ films displayed strong intensity dependence in their decay dynamics, indicative of bimolecular recombination. The Langevin bimolecular recombination rate[49] is 2.4×10^{-10} cm^3 s^{-1} for PDBT-T1:SdiPBI-Se, slightly higher than 1.6×10^{-10} cm^3 s^{-1} for PDBT-T1:$PC_{70}BM$ as determined by curve fitting from data in Figure 4b. Overall the maximum photocarrier population signals are roughly the same for PDBT-T1:SdiPBI-Se and PDBT-T1:$PC_{70}BM$ (Figure S10), consistent with the cell performance and that both devices show comparable J_{sc}, and the relatively lower FF observed in PDBT-T1:SdiPBI-Se solar cells is mainly ascribed to the stronger bimolecular recombination in films.

CONCLUSIONS

We have demonstrated that the introduction of selenium atoms into PBI core is an effective way to develop promising non-fullerene acceptors. The main absorption of SdiPBI-Se is in the wavelength range of 400−600 nm, complementary with the absorption spectrum of PDBT-T1 donor. High polymer crystallinity and favorable backbone orientation in BHJ films can facilitate efficient charge transport. Ultrafast charge generation process occurring in PDBT-T1:SdiPBI-Se films can potentially increase photocarrier generation. As a result, the PDBT-T1:SdiPBI-Se solar cell shows a high PCE of 8.4%, with a V_{oc} of 0.96 V, a J_{sc} of 12.49 mA cm^{-2}, and a high FF of 70.2%. The performance is even comparable to that of PDBT-T1:PCBM solar cells under similar device fabrication conditions. The faster bimolecular recombination observed in PDBT-T1:SdiPBI-Se films relative to that in PDBT-T1:$PC_{70}BM$ films suggests that there is still room for improvement in this new non-fullerene acceptor. Our results provide important progress for solution-processed non-fullerene organic solar cells and demonstrate that non-fullerene acceptors have significant potential for competition with those of fullerene derivatives.

ASSOCIATED CONTENT

Supporting Information

The Supporting Information is available free of charge on the ACS Publications website at DOI: 10.1021/jacs.5b11149.

Experimental details, synthesis and characterizations, device fabrication and characterizations, UV absorption and photoluminescence quenching spectra, cyclic voltammogram measurement, SCLC measurements, AFM images, and TAS spectra. (PDF)

AUTHOR INFORMATION

Corresponding Authors

*sunym@buaa.edu.cn

*wangzhaohui@iccas.ac.cn

Author Contributions

D.M. and D.S. contributed equally.

Notes

The authors declare no competing financial interest.

ACKNOWLEDGMENTS

This work was financially supported by the National Natural Science Foundation of China (NSFC) (nos. 51473009, 21225209, 91427303, 21190032, and 51273203), the International Science & Technology Cooperation Program of China (no. 2014DFA52820), the 111 project (B14009), the 973 Program (2012CB932903, 2014CB643502, and 2015CB856502), NSFC-DFG joint project TRR61, and the Chinese Academy of Sciences (XDB12010100). We gratefully acknowledge Prof. Y. Liu and Prof. G. Yu for the assistance with AFM measurements.

REFERENCES

(1) Sariciftci, N. S.; Smilowitz, L.; Heeger, A. J.; Wudl, F. *Science* **1992**, *258*, 1474−1476.

(2) Li, G.; Zhu, R.; Yang, Y. *Nat. Photonics* **2012**, *6*, 153−161.

(3) Lu, L.; Zheng, T.; Wu, Q.; Schneider, A. M.; Zhao, D.; Yu, L. *Chem. Rev.* **2015**, *115*, 12666−12371.

(4) Huo, L.; Liu, T.; Sun, X.; Cai, Y.; Heeger, A. J.; Sun, Y. *Adv. Mater.* **2015**, *27*, 2938−2944.

(5) Liu, Y.; Zhao, J.; Li, Z.; Mu, C.; Ma, W.; Hu, H.; Jiang, K.; Lin, H.; Ade, H.; Yan, H. *Nat. Commun.* **2014**, *5*, 5293.

(6) Liao, S.-H.; Jhuo, H.-J.; Yeh, P.-N.; Cheng, Y.-S.; Li, Y.-L.; Lee, Y.-H.; Sharma, S.; Chen, S.-A. *Sci. Rep.* **2014**, *4*, 6813.

(7) He, Z.; Zhong, C.; Su, S.; Xu, M.; Wu, H.; Cao, Y. *Nat. Photonics* **2012**, *6*, 591−595.

(8) Small, C. E.; Chen, S.; Subbiah, J.; Amb, C. M.; Tsang, S.-W.; Lai, T.-H.; Reynolds, J. R.; So, F. *Nat. Photonics* **2011**, *6*, 115−120.

(9) Vohra, V.; Kawashima, K.; Kakara, T.; Koganezawa, T.; Osaka, I.; Takimiya, K.; Murata, H. *Nat. Photonics* **2015**, *9*, 403−408.

(10) Lenes, M.; Shelton, S. W.; Sieval, A. B.; Kronholm, D. F.; Hummelen, J. C. K.; Blom, P. W. M. *Adv. Funct. Mater.* **2009**, *19*, 3002−3007.

(11) Ross, R. B.; Cardona, C. M.; Guldi, D. M.; Sankaranarayanan, S. G.; Reese, M. O.; Kopidakis, N.; Peet, J.; Walker, B.; Bazan, G. C.; Van Keuren, E.; Holloway, B. C.; Drees, M. *Nat. Mater.* **2009**, *8*, 208−212.

(12) Anctil, A.; Babbitt, C. W.; Raffaelle, R. P.; Landi, B. J. *Environ. Sci. Technol.* **2011**, *45*, 2353−2359.

(13) Po, R.; Bernardi, A.; Calabrese, A.; Carbonera, C.; Corso, G.; Pellegrino, A. *Energy Environ. Sci.* **2014**, *7*, 925−943.

(14) Würthner, F. *Chem. Commun.* **2004**, 1564−1579.

(15) Li, C.; Wonneberger, H. *Adv. Mater.* **2012**, *24*, 613−636.

(16) Dittmer, J. J.; Marseglia, E. A.; Friend, R. H. *Adv. Mater.* **2000**, *12*, 1270−1274.

(17) Kozma, E.; Catellani, M. *Dyes Pigm.* **2013**, *98*, 160−179.

(18) Zhan, X.; Facchetti, A.; Barlow, S.; Marks, T. J.; Ratner, M. A.; Wasielewski, M. R.; Marder, S. R. *Adv. Mater.* **2011**, *23*, 268−284.

(19) Jiang, W.; Li, Y.; Wang, Z. *Acc. Chem. Res.* **2014**, *47*, 3135−3147.

(20) Jiang, W.; Li, Y.; Wang, Z. *Chem. Soc. Rev.* **2013**, *42*, 6113−6127.

(21) Ball, M.; Zhong, Y.; Wu, Y.; Schenck, C.; Ng, F.; Steigerwald, M.; Xiao, S.; Nuckolls, C. *Acc. Chem. Res.* **2015**, *48*, 267−276.

(22) Guo, X.; Facchetti, A.; Marks, T. J. *Chem. Rev.* **2014**, *114*, 8943−9021.

(23) Li, H.; Hwang, Y. J.; Courtright, B. A. E.; Eberle, F. N.; Subramaniyan, S.; Jenekhe, S. A. *Adv. Mater.* **2015**, *27*, 3266−3272.

(24) Zhong, Y.; Trinh, M. T.; Chen, R.; Wang, W.; Khlyabich, P. P.; Kumar, B.; Xu, Q.; Nam, C.-Y.; Sfeir, M. Y.; Black, C.; Steigerwald, M.

DOI: 10.1021/jacs.5b11149
J. Am. Chem. Soc. XXXX, XXX, XXX−XXX

L.; Loo, Y.-L.; Xiao, S.; Ng, F.; Zhu, X.-Y.; Nuckolls, C. *J. Am. Chem. Soc.* **2014**, *136*, 15215−15221.
(25) Zhao, J.; Li, Y.; Lin, H.; Liu, Y.; Jiang, K.; Mu, C.; Ma, T.; Lin Lai, J. Y.; Hu, H.; Yu, D.; Yan, H. *Energy Environ. Sci.* **2015**, *8*, 520−525.
(26) Lin, Y.; Wang, J.; Zhang, Z. G.; Bai, H.; Li, Y.; Zhu, D.; Zhan, X. *Adv. Mater.* **2015**, *27*, 1170−1174.
(27) Zhong, Y.; Trinh, M. T.; Chen, R.; Purdum, G. E.; Khlyabich, P. P.; Sezen, M.; Oh, S.; Zhu, H.; Fowler, B.; Zhang, B.; Wang, W.; Nam, C.-Y.; Sfeir, M. Y.; Black, C. T.; Steigerwald, M. L.; Loo, Y.-L.; Ng, F.; Zhu, X.-Y.; Nuckolls, C. *Nat. Commun.* **2015**, *6*, 8242.
(28) Lin, H.; Chen, S.; Li, Z.; Lai, J. Y. L.; Yang, G.; McAfee, T.; Jiang, K.; Li, Y.; Liu, Y.; Hu, H.; Zhao, J.; Ma, W.; Ade, H.; Yan, H. *Adv. Mater.* **2015**, *27*, 7299−7304.
(29) Lin, Y.; Li, Y.; Zhan, X. *Chem. Soc. Rev.* **2012**, *41*, 4245−4272.
(30) Hwang, Y. J.; Courtright, B. A. E.; Ferreira, A. S.; Tolbert, S. H.; Jenekhe, S. A. *Adv. Mater.* **2015**, *27*, 4578−4584.
(31) Zhou, E.; Cong, J.; Hashimoto, K.; Tajima, K. *Adv. Mater.* **2013**, *25*, 6991−6996.
(32) Zhou, Y.; Kurosawa, T.; Ma, W.; Guo, Y.; Fang, L.; Vandewal, K.; Diao, Y.; Wang, C.; Yan, Q.; Reinspach, J.; Mei, J.; Appleton, A. L.; Koleilat, G. L.; Gao, Y.; Mannsfeld, S. C. B.; Salleo, A.; Ade, H.; Zhao, D.; Bao, Z. *Adv. Mater.* **2014**, *26*, 3767−3772.
(33) Sun, D.; Meng, D.; Cai, Y.; Fan, B.; Li, Y.; Jiang, W.; Huo, L.; Sun, Y.; Wang, Z. *J. Am. Chem. Soc.* **2015**, *137*, 11156−11162.
(34) Ballantyne, A. M.; Chen, L.; Nelson, J.; Bradley, D. D. C.; Astuti, Y.; Maurano, A.; Shuttle, C. G.; Durrant, J. R.; Heeney, M.; Duffy, W.; McCulloch, I. *Adv. Mater.* **2007**, *19*, 4544−4547.
(35) Hollinger, J.; Jahnke, A. A.; Coombs, N.; Seferos, D. S. *J. Am. Chem. Soc.* **2010**, *132*, 8546−8547.
(36) Patra, A.; Wijsboom, Y. H.; Zade, S. S.; Li, M.; Sheynin, Y.; Leitus, G.; Bendikov, M. *J. Am. Chem. Soc.* **2008**, *130*, 6734−6736.
(37) Oyaizu, K.; Iwasaki, T.; Tsukahara, Y.; Tsuchida, E. *Macromolecules* **2004**, *37*, 1257−1270.
(38) Earmme, T.; Hwang, Y.-J.; Murari, N. M.; Subramaniyan, S.; Jenekhe, S. A. *J. Am. Chem. Soc.* **2013**, *135*, 14960−14963.
(39) Malliaras, G. G.; Salem, J. R.; Brock, P. J.; Scott, C. *Phys. Rev. B: Condens. Matter Mater. Phys.* **1998**, *58*, R13411.
(40) Tan, L.; Jiang, W.; Jiang, L.; Jiang, S.; Wang, Z.; Yan, S.; Hu, W. *Appl. Phys. Lett.* **2009**, *94*, 153306.
(41) Müller-Buschbaum, P. *Adv. Mater.* **2014**, *26*, 7692−7709.
(42) Kaake, L. G.; Jasieniak, J. J.; Bakus, R. C.; Welch, G. C.; Moses, D.; Bazan, G. C.; Heeger, A. J. *J. Am. Chem. Soc.* **2012**, *134*, 19828−19838.
(43) Kaake, L. G.; Moses, D.; Heeger, A. J. *J. Phys. Chem. Lett.* **2013**, *4*, 2264−2268.
(44) Kaake, L. G.; Zhong, C.; Love, J. A.; Nagao, I.; Bazan, G. C.; Nguyen, T.-Q.; Huang, F.; Cao, Y.; Moses, D.; Heeger, A. J. *J. Phys. Chem. Lett.* **2014**, *5*, 2000−2006.
(45) Gélinas, S.; Rao, A.; Kumar, A.; Smith, S. L.; Chin, A. W.; Clark, J.; van der Poll, T. S.; Bazan, G. C.; Friend, R. H. *Science* **2014**, *343*, 512−516.
(46) Zhong, C.; Choi, H.; Kim, J. Y.; Woo, H. Y.; Nguyen, T. L.; Huang, F.; Cao, Y.; Heeger, A. J. *Adv. Mater.* **2015**, *27*, 2036−2041.
(47) Hoke, E. T.; Vandewal, K.; Bartelt, J. A.; Mateker, W. R.; Douglas, J. D.; Noriega, R.; Graham, K. R.; Fréchet, J. M. J.; Salleo, A.; McGehee, M. D. *Adv. Energy Mater.* **2013**, *3*, 220−230.
(48) Rao, A.; Chow, P. C.; Gélinas, S.; Schlenker, C. W.; Li, C.-Z.; Yip, H.-L.; Jen, A. K.-Y.; Ginger, D. S.; Friend, R. H. *Nature* **2013**, *500*, 435−439.
(49) Kaake, L. G.; Sun, Y.; Bazan, G. C.; Heeger, A. J. *Appl. Phys. Lett.* **2013**, *102*, 133302.

DOI: 10.1021/jacs.5b11149
J. Am. Chem. Soc. XXXX, XXX, XXX−XXX